IASMiRT

SMiRT 26
50 Anniversary Berlin/Potsdam

Transactions, SMiRT-26
Berlin/Potsdam, Germany, July 10-15, 2022
Division VI

APPLICATION OF DEFORMATION INDEX OF SHEAR FAILURE FOR SEISMIC PERFORMANCE VERIFICATION TO FULL-SCALE RC MEMBER SUBJECTED TO HORIZONTAL BILATERAL LOADING

Satoshi Komatsu[1], Yoshinori Miyagawa[2] and Toyofumi Matsuo[2]

[1] Research scientist, Central Research Institute of Electric Power Industry, Japan
(komatsu3762@criepi.denken.or.jp)
[2] Senior research scientist, Central Research Institute of Electric Power Industry, Japan

ABSTRACT

For the purpose of advancing and rationalizing the seismic performance verification method using the three-dimensional material nonlinear finite element method, in this paper, the applicability of the limit value index "thickness increment of RC member" assumed in out-of-plane shear failure has been verified in full-scale RC members with shear failure subjected to bilateral loading. First, using the experimental results of full-scale RC pillar members that failed in shear due to two loading patterns (N-1: horizontal one-directional load applied, N-2-1: horizontal bilateral loading applied simultaneously), analytical models with different element dimensions were validated. Then, the applicability of the index was verified. Next, as case studies, the influence of the calculation method of the index on the evaluation results was investigated, and analytical models without shear reinforcing bars were created and the applicability of the index was verified. Finally, the applicability of the index to RC members in different paths of horizontal bilateral loading was verified by newly creating analysis case “N-3” in which horizontal bidirectional loading is applied in sequence.

As a result, within the scope of this study, the index was found to roughly estimate the failure mode and its degree regardless of the loading paths under horizontal bilateral loading. Furthermore, the index was found to allow more rational evaluation of the load carrying capacity than the design equation, with small element size dependence. Another finding is that when the horizontal bilateral loading acts simultaneously, it is safer to calculate the index by using the distance change between nodes in the resultant load direction.

INTRODUCTION

For confirming the seismic safety of concrete structures, verification methods using numerical analysis are becoming widely used. For RC underground structures that constitute the emergency cooling facility of a nuclear power plant, as shown in **Figure 1**, non-linear time-dependent analysis considering integrated mechanical behavior of the ground and the structures has become the standard evaluation method (Nuclear Civil Engineering Committee (2021)). In particular, since the shear failure of RC members progresses in a brittle manner, accurate estimation through numerical analysis is desirable. Therefore, as an index of shear failure, the authors have proposed the "thickness increment of RC member", which is an index related to the change in thickness of an RC member before and after damage. This index is mainly intended to be used for seismic performance verification of RC members such as walls, slabs, and columns, which are constituent members of underground structures. However, in the studies done so far, applicability verification in full-scale RC members has not been sufficient.

The background to the proposal of this index is that the limit value index using strain (for example, principal compressive strain and principal tensile strain) generally has element size dependence. In addition, the required performance of RC underground structures is that they do not fail against the standard ground

motion. In general, the design equation is formulated with a safety margin, and this might result in an excessively conservative evaluation (seismic performance verification) when applied to RC underground structures. Based on the above, in this study, the validity of the numerical analysis model was confirmed by using the experimental results of full-scale RC members with shear failure due to horizontal bilateral loading, and the applicability of the index was confirmed under various conditions assumed in the service environment.

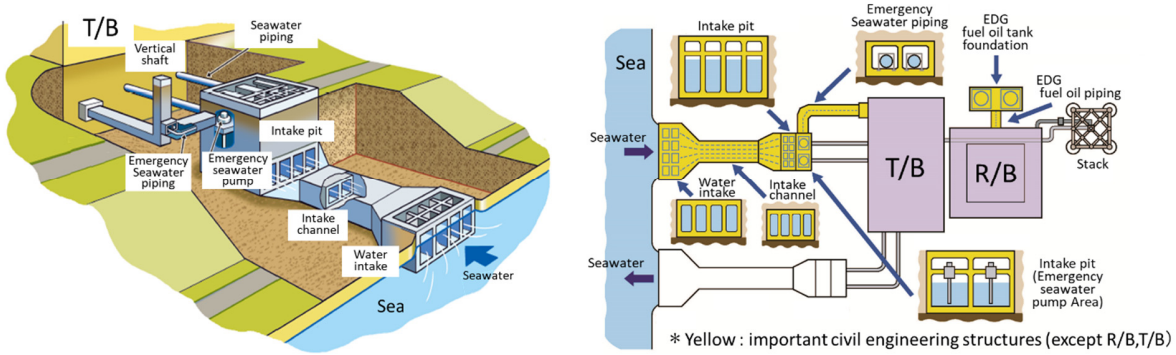

Figure 1. Underground structures in nuclear power station.

DEFINITION OF THE INDEX

"Thickness increment of RC member", which indicates the amount of expansion in the thickness direction of the member, as shown in Eq. (1), is mainly composed of diagonal cracks (X-shaped cracks) and bond splitting cracks, and roughly corresponds to the total of those openings. It can be applied to both one-way and repetitive loadings.

$$\Delta D_{lim} = max\{5,\ 2.5 p_w D\} \tag{1}$$

where ΔD_{lim} is the limit value of thickness increment of the RC member [mm], p_w is the shear reinforcement ratio, and D is the member thickness [mm].

Figure 2 shows the image of the nodes used in the calculation. It is effective as an evaluation index for out-of-plane shear failure because it does not detect the opening of bending cracks but detects the opening of diagonal shear cracks.

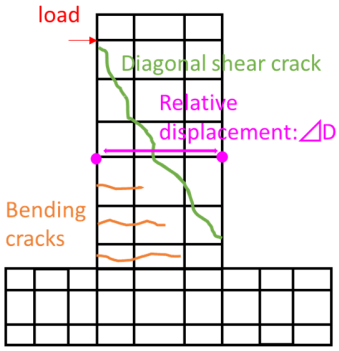

Figure 2. Image of thickness increment of RC member.

The first term (5 mm) focuses on members without out-of-plane shear reinforcing bars. According to previous experiments with member thicknesses of 400 to 800 mm and an axial force ratio of -0.05 to 0.05, the residual rate of load carrying capacity in the direction perpendicular to the member axis is 60% to

95% when there is an expansion of 5 mm in the thickness direction, as reported by Miyagawa et al. (2014). In addition, Chi et al. (2018) reported that according to the results of beam analysis by RBSM (Rigid Body Spring Model), which is good at evaluating crack width, an oblique crack width of about 4 to 6 mm occurred at the maximum shear stress.

The second term ($2.5p_wD$) considers the distribution of cracks due to the use of shear reinforcing bars. As a result of analytical case studies, the relationship shown in Eq. (2) was found in members with different specimen lengths, reinforcing bar ratios, and reinforcing bar diameters.

$$\varepsilon_{ave} = 2.5p \tag{2}$$

where ε_{ave} is the average strain and p is the reinforcing bar ratio (direct value not expressed in %). The displacement index is obtained by multiplying average strain ε_{ave} by member thickness D.

In past studies by Miyagawa et al. (2014) and (2018), applicability of the index when a load acts on a full-scale member in one horizontal direction and when a load acts on a small-scale specimen in bilateral horizontal directions has been verified. However, applicability when the load acts on the full-scale members in horizontal bilateral directions has not been sufficiently verified. Regarding the calculation method of the index, the change in the distance between nodes at the same height facing each other in the loading direction can be used for RC members subjected to a one-directional load. However, in the case of three-dimensional deformation behavior as in this study, it is necessary to confirm the effect of the calculation method on the evaluation results as shown in **Figure 3**.

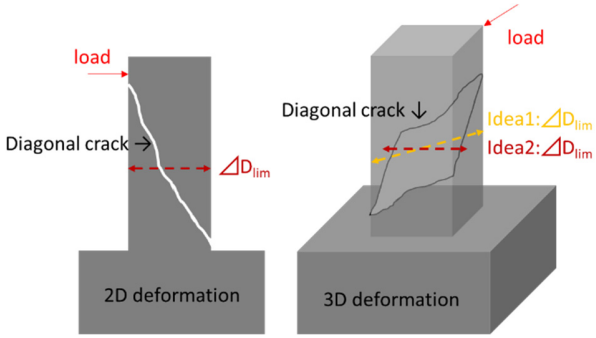

Figure 3. Image of thickness increment of RC member in 2D and in 3D.

EXPERIMENTAL SETUP

SPECIMEN DETAILS

Table 1 shows the types of experimental cases. The box culvert mainly consists of walls, but due to the restrictions of the experimental equipment, pillar members with footing were cast. The reinforcing bar arrangement of the N-1 and N-2-1 cases were the same, and they were designed to shear failure. The difference between the two cases is the difference in the loading pattern, which is described later. One specimen was cast for each case. **Figure 4** shows the

Table 1: Case names.

Case name	Reinforcement ratio [%]		Fracture behavior	Loading age [days]
	Main rebar	Shear rebar		
N-1	1.58	0.08	Diagonal cracks	82
N-2-1				97

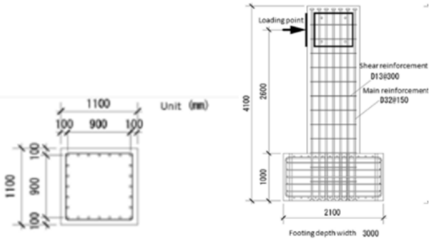

Figure 4. Overview of specimen.

dimensions and reinforcing bar arrangement of the specimen. The facing surfaces of the loading plates on which the 3MN jacks are installed are tense with PC steel rods.

MATERIALS

Table 2 shows the physical properties of the concrete. The tensile strength was calculated by using the compressive strength derived from the report by the Concrete Committee (2018). **Table 3** shows the physical properties of the reinforcing bars.

Table 2: Material properties of concrete.

Case Name	Compressive strength [N/mm^2]	E modulus [kN/mm^2]	Tensile strength [N/mm^2]
N-1	36.9	30.0	2.5
N-2-1	39.1	30.8	2.6

Table 3: Material properties of reinforcing bar.

	Yielding strength [N/mm^2]	Tensile strength [N/mm^2]	E modulus [kN/mm^2]
Main rebar (D32)	508	676	196
Shear rebar (D13)	360	476	188

LOADING SETUP AND LOADING PATTERN

The loading setup is shown in **Figure 5**. By using two jacks, it is possible to apply loadings to the specimen in various directions. The loading pattern is shown in **Figure 6**. The "□" shape in that figure is an image diagram of the pillar viewed from directly above.

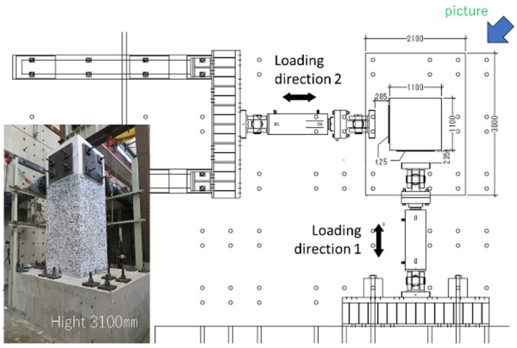

Figure 5. Overview of loading setup.

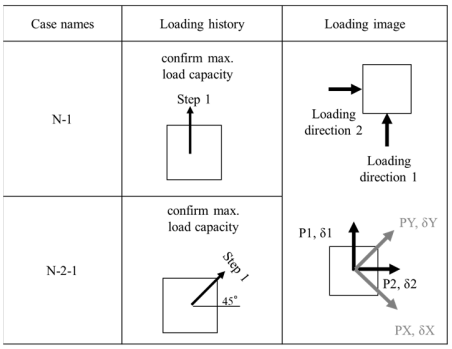

Figure 6. Loading patterns of each specimen.

MEASURING POINTS

Horizontal displacements were measured at the loading point position (2,600 mm) and at the center of the column height (1,300 mm). In order to measure the deformation of the entire column, in other words, measure the thickness increment of RC member due to diagonal cracks, motion captures were placed at the angle of the column and 6 points in the height direction, for a total of 24 points, on the wall surface 24 mm inside from the corner. The thickness increment of the RC member was calculated from the change in distance between motion captures at the same height.

OUTLINE OF ANALYSIS

In this study, a three-dimensional material nonlinear finite element method analysis program (COM3) was used. This is an analysis program that extends the RC plane model based on the material nonlinear

constitutive law corresponding to an arbitrary loading history in three dimensions. This program shows high analysis accuracy, as reported by Maekawa et al. (2003). The RC plane model defines the average strain-stress relationship by averaging the behavior of multiple fine cracks in a finite volume (smeared crack model). The average strain-stress relationship of concrete consists of one-dimensional compression, tension, and shear transfer models of cracked surfaces, each of which is time dependent. By using the multi-directional non-orthogonal fixed crack model, it is possible to estimate the occurrence of multi-directional multiple cracks and the behavior after crack occurrence according to the loading history.

Regarding the RC constitutive law, by dividing the elements in consideration of the reinforcing bar ratio, the direction of the reinforcing bars, and the arrangement of the reinforcing bars, the strain hardening (restraining effect) of the concrete by the reinforcing bars can be considered before the occurrence of cracks. On the other hand, after cracks occur, the tensile stiffening model, which considers the bonding between the reinforcing bar and concrete on a spatial average, is applied to the tensile region of the RC element, as shown in Eq. (3).

$$\sigma = R_f f_t \left(\frac{\varepsilon_{tu}}{\varepsilon}\right)^c \tag{3}$$

where σ is the tensile stress, R_f is the tensile strength reduction coefficient, ε is the tensile strain, ε_{tu} is the crack generation strain, and c is a constant value representing bonding properties.

On the other hand, for plane concrete element, the tensile softening model obtained from the fracture energy and element dimensions is given by Eq. (4).

$$\int_{\varepsilon_{tu}}^{\varepsilon_{te}} \sigma d\varepsilon + \frac{1}{4} f_t \varepsilon_{tu} = \frac{G_f}{l} \tag{4}$$

where ε_{te} is the ultimate tensile strain, G_f is the fracture energy, and l is the element size.

MESH DIVISIONS

Figure 7 shows the state of element division. In order to verify the element size dependence of the index, two analysis models with different element dimensions were created. Unless otherwise specified in this paper, an analytical model with large element dimensions is used.

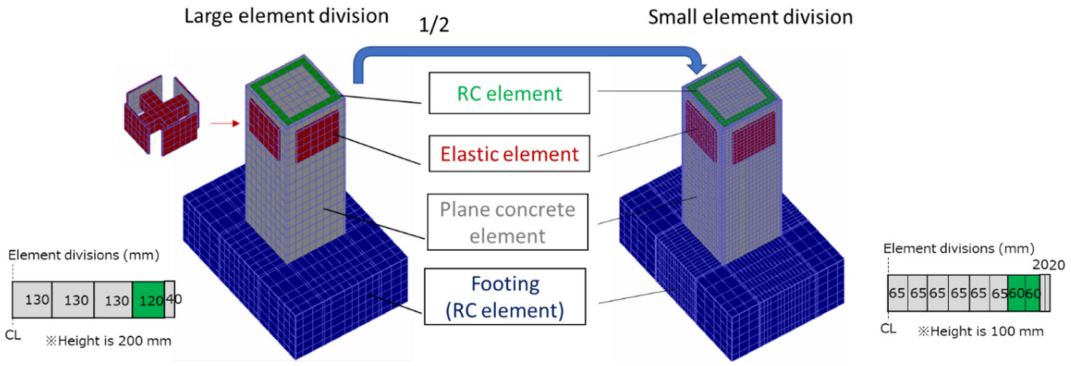

Figure 7. Element division of specimen.

In order to properly consider the effect of bonding between the reinforcing bar and concrete regardless of the element size, the main reinforcing bar was placed at the center of the RC element cross section. A plane concrete element was placed in the area where the bonding does not reach. Shear-reinforcing bars are treated as being uniformly distributed in the RC element (constant reinforcing bar ratio). Since the loading plate installed on the specimen is fixed with PC bars, the concrete is not stressed by

pushing and pulling the jacks. In this model, the situation was reproduced by connecting the loading plates to each other with elastic elements for convenience.

INPUT DATA

Basically, the results of the material test were used as is. Regarding the tensile strength of concrete, the analysis accuracy is described in Nuclear Civil Engineering Committee (2021) to have been improved by reducing the apparent tensile strength because of the shrinkage stress generated on the concrete surface due to drying shrinkage, etc. In this study, the tensile strength was reduced to 60%. The tensile stiffening coefficient in RC elements was 0.4 in the main reinforcing bar axial direction, 0.8 in the shear reinforcing bar direction, and 2.0 in the reinforcing bar orthogonal direction, respectively. The tensile softening coefficient in plane concrete elements was determined according to the element dimensions.

VALIDATION OF ANALYTICAL MODEL AND APPLICABILITY OF INDEX

Case N-1

Figure 8 shows the deformation behavior of N-1 at the maximum load capacity. The experimental values (the average of the two measured values) obtained by motion captures are described by points, and the analysis results are described by solid lines. In addition, the limit value (5 mm) is shown by the red line.

The analysis results are greatly increased near the height of about 200 mm from the footing. It is considered that this is because, as shown in the maximum principal strain contour diagram and the state of failure of the specimen, bond splitting cracks occurred at the base of the column, where the cover concrete is spalled. In other words, the analysis results can roughly estimate the deformation behavior of the specimen.

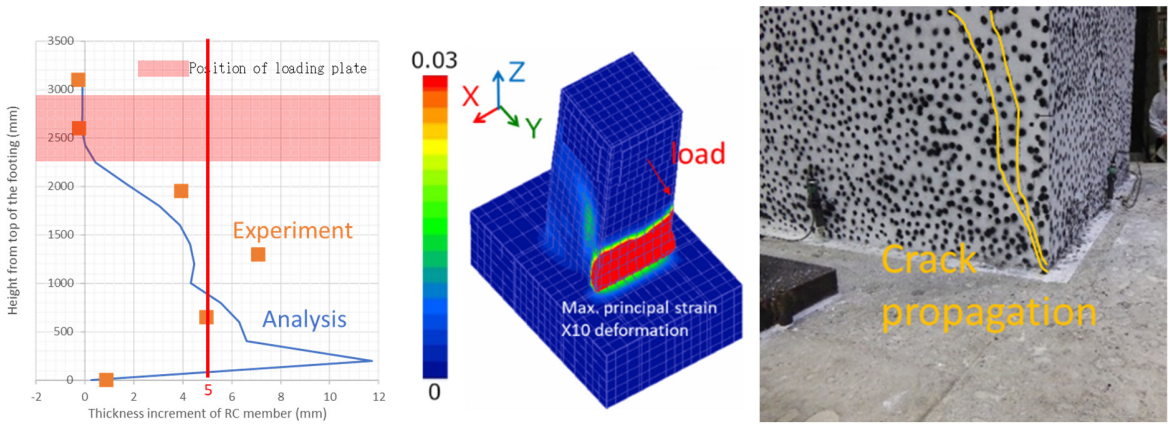

Figure 8. Deformation behavior at maximum load capacity (N-1).

Figure 9 shows the load-displacement relationship and the time-dependent change of the index using two analytical models with different element dimensions. The point where the index reaches the limit value is indicated by "○" on the load-displacement relationship, and the load carrying capacity calculated by the design equation (Concrete Committee (2018)) is also shown. It can be mentioned that the estimation accuracy of the analysis model is high because the analysis results and the experimental results are almost the same up to the maximum load capacity. In addition, regardless of the element dimensions, the limit value was reached with approximately the same load capacity (98-99% of maximum load capacity). Therefore, it was confirmed that a rational evaluation is possible from the design equation.

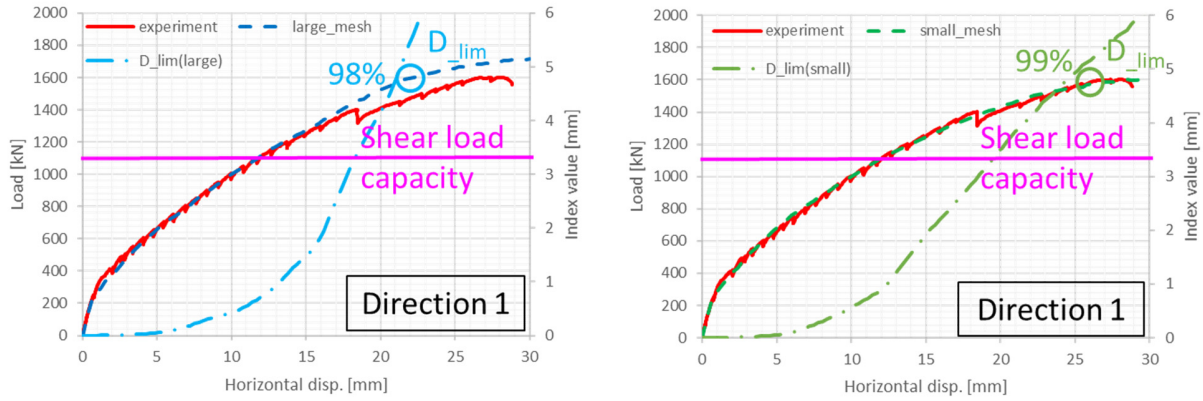

Figure 9. Load-disp. relationship and time-dependent change of index (N-1).

Case N-2-1

Figure 10 shows the deformation behavior of N-2-1 at the maximum load capacity. The experimental values (the average of the two measured values) obtained by motion capture are shown by points, and the analysis results are shown by solid lines. The limit value (5 mm) is also shown by the red line.

The large values of the analysis results near the height of 200 mm are considered to be due to bond splitting cracks, as described above. Since the maximum principal strain contour diagram and the failure conditions of the specimen are very similar, the analysis results can roughly estimate the deformation behavior of the specimen in this case as well.

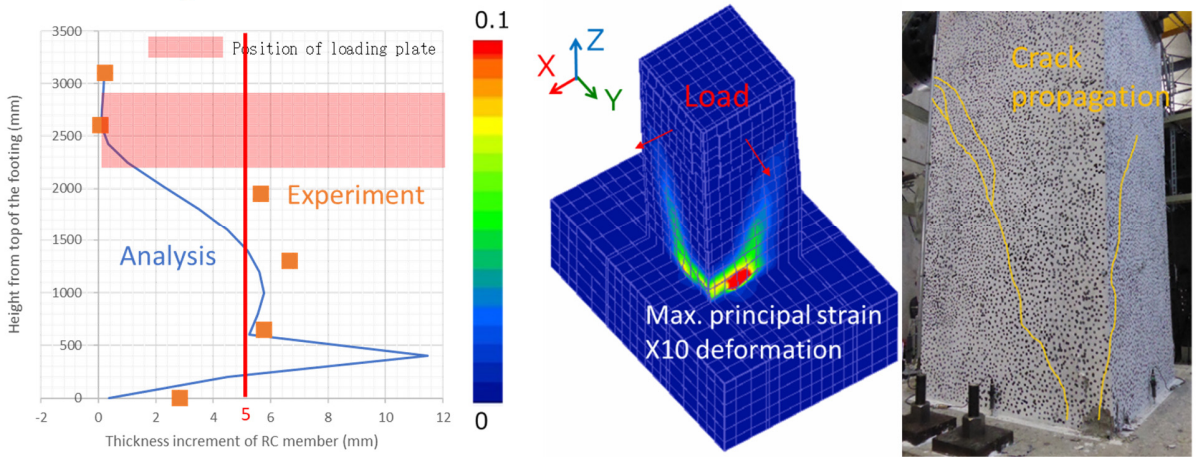

Figure 10. Deformation behavior at maximum load capacity (N-2-1).

Figure 11 shows the load-displacement relationship and the time-dependent changes of the index using two analytical models with different element dimensions. The point where the limit value is reached is indicated by "○" on the load-displacement relationship, and the load carrying capacity calculated by the design equation (Concrete Committee (2018)) is also shown. Here, as shown for Idea 1 in **Figure 3**, the distance between the nodes in the resultant loading direction is used in the calculation of the index. It can be mentioned that the estimation accuracy of the analysis model is high because the analysis results and the experimental results are almost the same up to the maximum load capacity. In addition, regardless of the element dimensions, the limit value was reached with approximately the same load capacity (98-99% of maximum load capacity). Therefore, it was confirmed that a rational evaluation is possible from the design equation.

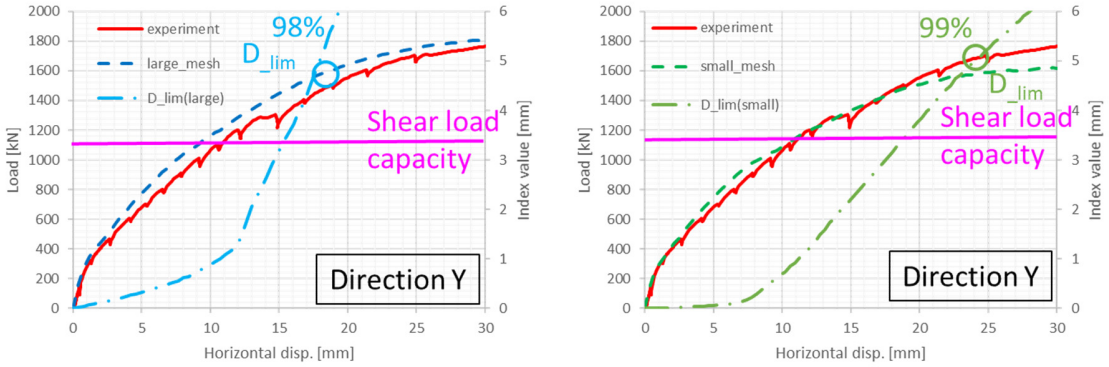

Figure 11. Load-disp. relationship and time-dependent change of the index (N-2-1).

CASE STUDY

Influence of Calculation Method on Evaluation Result

Here, the effect of the calculation method on the evaluation results is discussed. The calculation method is as indicated in **Figure 3**.

Figure 12 shows the results for N-2-1. It was found that when the distance between nodes is calculated in the resultant loading direction, the evaluation can be performed on the safe side instead of calculating the distance between nodes facing each other at the same height. However, even if the distance between nodes facing each other at the same height was used in the calculation, the evaluation results did not change significantly.

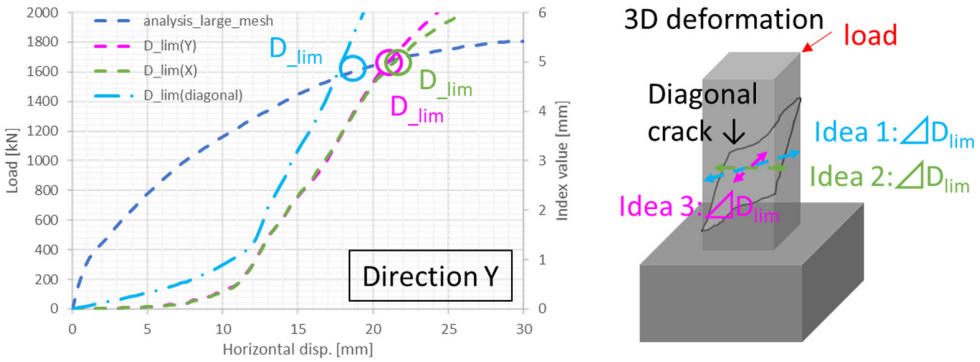

Figure 12. Load-disp. relationship and time-dependent change of index (N-2-1).

Effect of Shear Reinforcement on Evaluation Result

To verify applicability to full-scale members, it is necessary to study the case where there is no shear reinforcing bar, which is considered to show more brittle failure. Therefore, in this section, an analysis model excluding the shear reinforcing bars was created, and the applicability of the index has been verified.

Figure 13 shows the load-displacement relationship and time-dependent change of the index for N-1 and N-2-1 without shear reinforcing bars. The failure mode was diagonal tensile failure. Since there is no shear reinforcing bar, the maximum load capacity is lower than that with the shear reinforcing bar. However, in both cases, the index reached the limit value at almost the maximum load carrying capacity (95-98%). That is because the cross-sectional area of concrete, which contributes to the shear strength, has increased due to massive members. It is concluded that the index can be applied not only when a full-scale RC member has shear reinforcing bars but also when it does not.

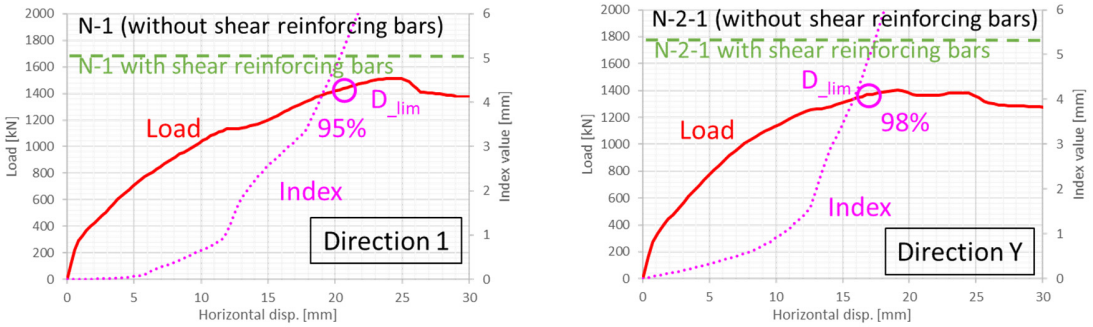

Figure 13. Load-disp. relationship and time-dependent change of index without shear reinforcing bars.

Effect of Loading Path of Bilateral Loading on Evaluation Result

Finally, applicability of the index to RC members with shear failure due to horizontal bilateral loading in different loading paths has been verified.

For this study, analysis case N-3, in which horizontal bidirectional loading is applied in sequence, was created. The loading path is shown in **Figure 14**. In N-3, loading is performed in Step 1 and Step 2 until the displacement of 18 mm in the diagonal 45 degrees direction when the index reaches the limit value in N-2-1. Then, in Step 3, loading is performed in the Y direction until the maximum load capacity is reached.

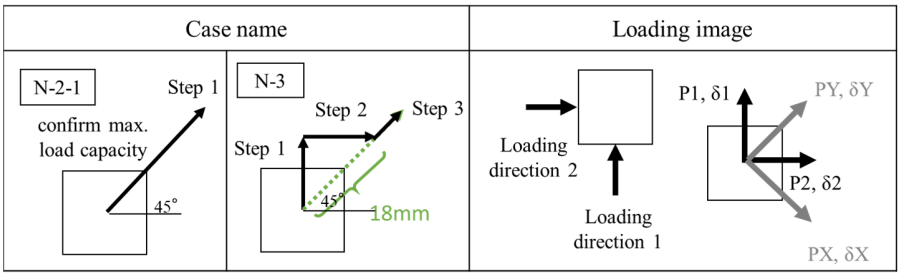

Figure 14. Loading path in N-2-1 and N-3.

Figure 15 shows the load-displacement relationship and the points where the index reached the limit value in N-3. In this analysis case, the direction of the resultant force changes sequentially, so the index was calculated using the change in distance between nodes at the same height facing each other.

As a result, it was found that the index reached the limit value first in loading direction 1 in the middle of Step 2. Even in loading direction 2, the index reached the limit value during the loading in Step 2. In other words, it was found that the index reaches the limit value with a smaller displacement than N-2-1, in which loadings are applied simultaneously in two horizontal directions.

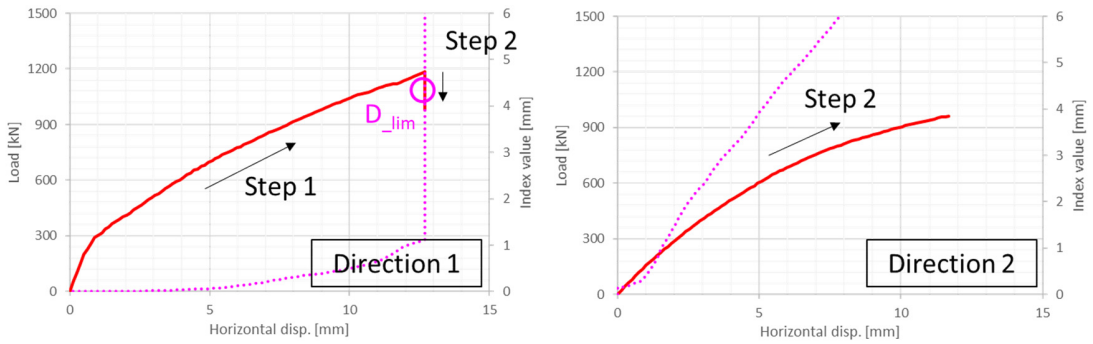

Figure 15. Load-disp. relationship and time-dependent change of index (N-3).

Table 4 shows the maximum load capacity of N-2-1 and N-3 when loading is applied in the Y direction. It was found that the maximum load capacity of N-3 was smaller than that of N-2-1. Maruyama et al. (1979) reported that RC column members are more severely damaged when they are sequentially loaded in two horizontal directions than when they are simultaneously loaded in two horizontal directions. This index shows the same tendency. **Figure 16** shows the contour diagram of the maximum principal strain when the index reaches the limit value. Spalling occurs in cover concrete at the base of the column, which would be the reason why the index reached the limit value.

Table 4: Maximum load capacity in case of N-3 and N-2-1.

Case name	Loading step (in Figure 14)	Maximum load capacity [kN]
N-2-1	1	1806
N-3	3	1631

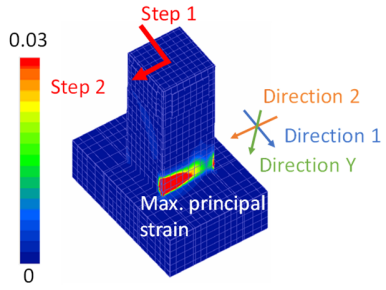

Figure 16. Maximum principal strain when the index reaches limit (N-3).

CONCLUSIONS

In this paper, the applicability of the "thickness increment of RC member", which is a limit value index assuming out-of-plane shear failure, has been verified by using full-scale RC members with shear failure under bilateral loading. The results of this study are summarized below.

(1) The failure mode and its degree can be roughly estimated by the index regardless of whether the horizontal bilateral loading acts simultaneously or sequentially on the full-scale RC member.
(2) The index was able to evaluate the load carrying capacity more rationally than the design equation, and the element size dependence was small. In the experimental conditions, the index reached the limit value at 98-99% of the maximum load capacity in the RC member. On the other hand, in full-scale members without shear reinforcing bars, the index reached the limit value when the load capacity reached 95-98% of the maximum load capacity in this study.
(3) In the full-scale RC members subjected to horizontal bilateral loading simultaneously, it is safer to calculate the index in the resultant loading direction. However, even if the index is calculated using the distance between nodes at the same height facing each other, the evaluation result is not much different.

REFERENCES

Chi S., Nakamura H., Yamamoto Y., Miura T.: Examination of effect of shear reinforcement on size effect of shear strength in RC beam, Proceedings of the Japan Concrete Institute, Vol. 40, No. 2, pp. 619-624, 2018. (in Japanese)

Concrete Committee, JSCE: Standard specifications for concrete structures – Design, 2018. (in Japanese)

Nuclear Civil Engineering Committee, JSCE: Safety Evaluation Manual for Earthquake Resistant Design of Important Civil Engineering Structures in Nuclear Power Plants 2021, 2021.10. (in Japanese)

Maekawa, K., Pimanmas, A. and Okamura, H.: Nonlinear Mechanics of Reinforced Concrete, Taylor & Francis Group, Spon Press. 2003.

Maruyama, K. and Jirsa, J. O.: Shear Behavior of Reinforced Concrete Members under Bidirectional Reversed Lateral Loading, CESRL Report, No. 79-1, The University of Texas at Austin, Aug. 1979.

Miyagawa, Y., Nagata, S. and Matsumura, T.: Lateral Expansion and residual load capacity of reinforced concrete members without transverse reinforcement, Journal of Japan Society of Civil Engineers, Ser. E2 (Materials and Concrete Structures), Vol. 70(4), pp. 402-416, 2014. (in Japanese)

Miyagawa, Y., Shibayama, A., Morozumi, H. and Shigemitsu, N.: Entire Displacement Distribution of Reinforced Concrete Box Culvert in the Damaging Progress Subjected to Horizontal Load, Proceedings for the 2018 fib Congress, Melbourne, pp. 626-645, 2018.